Visualization of Vesicle Transport Along and Between Distinct Pathways in Neurites of Living Cells

GERHARD J. SCHÜTZ,[1]* MARKUS AXMANN,[1] SUSANNE FREUDENTHALER,[1] HANSGEORG SCHINDLER,[1] KOSTYA KANDROR,[2] JOHN C. RODER,[3] AND ANDREAS JEROMIN[4]
[1]*Institute for Biophysics, University of Linz, A-4040 Linz, Austria*
[2]*Department of Biochemistry, Boston University School of Medicine, Boston, Massachusetts 02218*
[3]*Mt. Sinai Hospital, SRLI, Toronto, Ontario, M5G1X5 Canada*
[4]*Division of Neuroscience, Baylor College of Medicine, Houston, Texas 77030*

KEY WORDS fluorescence microscopy; vesicle tracking; 3D imaging; microtubule; motor molecules; vesicle sorting

ABSTRACT Trafficking of secretory vesicles along neurites of PC12 cells was visualized by 2D and 3D real-time imaging using fluorescence microscopy. Vesicle motion along distinct pathways was directly seen. From an overlay of individual pathways, the underlying cytoskeletal filament could be imaged at a subwavelength resolution. Continuous vesicle transport was interrupted by periods of diffusive motion with concomitant pathway changes. Statistical analysis shows that such interruptions were distributed stochastically along the filament, indicating a limited processivity of motor proteins also in a cellular context. Periods of diffusive motion facilitated the interaction with actively transported vesicles. Frequent associations and dissociations of vesicles have been observed consistently, pointing to a functional relevance of vesicle cotransport. *Microsc. Res. Tech. 63: 159–167, 2004.*

INTRODUCTION

Continuous supply of nutrients in cells is mediated via the transport of vesicles containing cargo, such as proteins and lipids, along distinct pathways, predominantly microtubules (Sheetz, 1999; Lippincott-Schwartz et al., 2000). In neuronal cells the transport machinery is thought to be optimized for fast delivery of vesicles from the cell body along neurites to sites of growth and communication, the growth cone and synapses (Allen et al., 1982; Brady et al., 1982; Kuznetsov et al., 1992; Lin and Scheller, 2000). Neurites contain microtubules, intermediate filaments, and actin filaments as the three major classes of cytoskeletal components (Kobayashi and Mundel, 1998). Transport relies on directed movement mediated by the two major types of microtubule-associated motor proteins, kinesin and dynein (Hirokawa, 1998). In neuronal cells the growth of microtubules is polarized, with the growing end directed to the processes, and with kinesin and dynein being responsible for anterograde and retrograde transport, respectively (Goldstein and Yang, 2000). Detailed information about motor protein motion along microtubules has been obtained in vitro in isolated systems (Vale and Milligan, 2000), yielding processive movements of individual kinesin or dynein molecules over distances of ~1.5 μm before dissociating from the microtubule (Block et al., 1990). Much less corresponding mechanistic information on transport velocity and processivity is available within living cells. There is currently no clear picture of how pathway changes occur, an important issue in view of the many pathway changes required for the long distance traveling from cell body to growth cone (Thorn et al., 2000). Indeed, the limited length of cytoskeletal filaments (Yu and Baas, 1994) and the existence of obstacles along the pathway renders changes of the transport route inevitable. It has been suggested that the observed low processivity (Thorn et al., 2000) may have evolved either to circumvent these obstacles or to achieve an optimum balance between vectorial transport and random motion (Taylor and Borisy, 2000). In addition, a recent study reported a more complex transport behavior of vesicles, with preassembly or en route assembly of larger vesicle associates, called prototerminals (Ahmari et al., 2000).

Here, we applied real-time 2D and 3D imaging (Schutz et al., 2000b) to resolve mechanistic details during transport of individual motor-driven vesicles. Secretory vesicles were imaged in stable transfected, differentiated neuroendocrine (PC12) cells. These cells share many features with neurons: they undergo calcium-dependent exocytosis (Meldolesi et al., 1984) and have been used to study the transport of secretory granules in real time (Lang et al., 1997; Lochner et al., 1998; Abney et al., 1999). VAMP-2 was fused to enhanced green fluorescent protein (VAMP-eGFP) and used as a tool to monitor its trafficking. Like nontagged VAMP-2, VAMP-eGFP labeled a variety of vesicles of different shapes and sizes (Fig. 1), in agreement with earlier results by Papini et al. (1995). The movement of individual vesicles along two- and three-dimensional

*Correspondence to: Gerhard J. Schütz, Institute for Biophysics, University of Linz, Altenbergerstr. 69, A-4040 Linz, Austria. E-mail: gerhard.schuetz@jku.at

Received 26 June 2003; accepted in revised form 6 November 2003

Contract grant sponsor: Austrian Federal Ministry of Science and Transport; Contract grant numbers: GZ 200.025/3-Pr/4/1998; GZ 200.027/3-Pr/2a/1998; Contract grant sponsor: Austrian Research Funds; Contract grant numbers: P12803-MED, P15053.

DOI 10.1002/jemt.20016

Published online in Wiley InterScience (www.interscience.wiley.com).

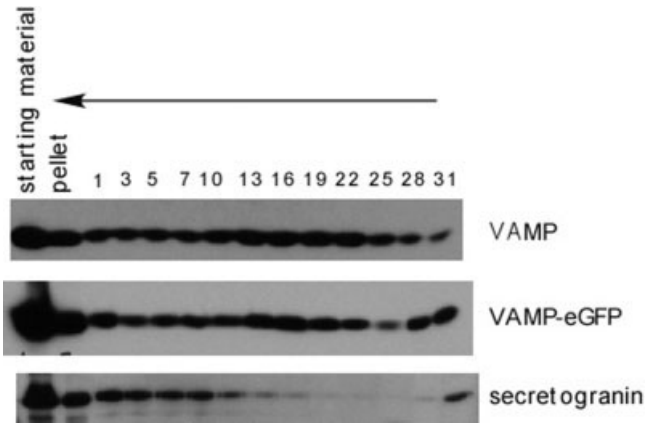

Fig. 1. Sedimentational distribution of VAMP-eGFP-containing vesicles in a sucrose velocity gradient. Cells were homogenized and a postnuclear supernatant (0.4 mg) was prepared as described in Materials and Methods. This material was fractionated in a 10–30% sucrose gradient for 50 minutes at 48,0000 rpm in an SW50.1 rotor. Equal volume aliquots of odd fractions were subjected to SDS-PAGE and individual proteins were detected by Western blot. The pellet of this centrifugation was resuspended in 250 μl of buffer A and analyzed along with gradient fractions. The arrow indicates the direction of sedimentation.

pathways was followed in time with an accuracy of 35 nm in the x- and y-direction and 75 nm in the z-direction (Schutz et al., 2000). The high positional accuracy obtained with this technique allowed us to gain mechanistic insights in vesicle transport at a resolution much below the diffraction limit of conventional light microscopy.

MATERIALS AND METHODS

Molecular Biology and Cell Culture

The VAMP-eGFP construct was generated by amplifying the rat VAMP2 cDNA (accession no. NM 012663) and subcloning it into pEGFPC1 (ClonTech, Palo Alto, CA). The integrity of the construct was confirmed by di-deoxysequencing. Several stable PC12 clones expressing VAMP-eGFP were generated following standard procedures (Scalettar, 2002). One of these clones (A1) was used for these experiments.

VAMP-eGFP PC12 cells were plated on gelatin-coated glass coverslips and treated with nerve growth factor (NGF, Boehringer, Mannheim, Germany) for 24–72 hours. For imaging experiments, these coverslips were mounted into a custom-made chamber and overlaid with phosphate-buffered saline (PBS). Experiments were performed at room temperature within 20 minutes after transfer to the microscope.

Fractionation of Membranes from PC12 Cells

Confluent 10 cm plates were rinsed twice at 4°C with buffer A (150 mM NaCl, 10 mM HEPES, pH 7.4, 1 mM EGTA, 0.1 mM $MgCl_2$). Cells were scraped into 1 ml buffer A in the presence of protease inhibitors (1 mM PMSF, 5 mM Benzamidine, 10 ng/ml each of aprotinin, pepstatin, and leupeptin) and homogenized with 10 strokes in a ball-bearing homogenizer (HGM Precision Engineering, Heidelberg, Germany) with a 12 μm clearance or in a Potter-Elvjeham homogenizer with a 12 μm clearance. The homogenate was centrifuged at 750*g* for 5 minutes and 200 μl of the resulting postnuclear supernatant was fractionated in a 10–30% (w/w) linear sucrose gradient. The sample was loaded at the top of the gradient and forced to float down. Gradients were prepared in buffer A and centrifuged for 50 minutes at 48,000 rpm in an SW50.1 rotor. Fractions were collected starting from the bottom of the gradient and analyzed for specific proteins by Western blot.

Gel Electrophoresis and Immunoblotting

Proteins were separated by SDS-PAGE according to Laemmli and transferred to an Immobilon-P membrane in 25 mM Tris, 192 mM glycine. Following transfer the membrane was blocked with 10% nonfat dry milk in PBS for 1 hour at 37°C and probed with specific antibodies to VAMP-2, eGFP, and secretogranin (Synaptic Systems, Goettingen, Germany).

Microscopy

The basic setup for fluorescence microscopy has been described previously (Schutz et al., 2000a). Here, cells were illuminated in an epifluorescence microscope (Axiovert 135TV, Zeiss) for 10 ms with 488 nm light from an Ar^+-ion Laser (Innova306, Coherent) at an intensity of typically 1 kW/cm^2. Fluorescence emission was imaged via an 100× objective (PlanNeofluar, NA = 1.3, Zeiss) and detected on an ultrasensitive liquid nitrogen-cooled CCD-camera (Micro Max 1300-PB, Roper Scientific, Tucson, AZ). An automatic analysis program determined the position of each vesicle to an accuracy of 35 nm by fitting the intensity profile to a 2D Gaussian surface with a diffraction-limited width.

For 3D imaging the basic setup was extended using a piezo-driven z-control of the objective (PIFOC, Physik Instrumente) (Schutz et al., 2000b). Individual 3D scans were performed at a delay of 10 ms between subsequent focal planes, while the delay between two successive scans was 200 ms. For each scan, four focal planes were recorded, separated by a distance dz = 500 nm. Each stack of images was fitted to the 3D pointspread function of the microscopic setup, as recorded on immobilized 30 nm fluorescent latex spheres.

RESULTS

For studying the trafficking of small synaptic-like microvesicles (SLMVs), stable PC12 clones expressing VAMP-2 eGFP were established and the distribution of VAMP-2 eGFP was characterized by subcellular distribution. In control experiments, we demonstrated that VAMP-2 eGFP represents a legitimate tool for the analysis of SLMV traffic, since its intracellular distribution mimics that of endogenous VAMP-2, an essential protein component of this compartment (Fig. 1). As seen in this figure, endogenous VAMP-2 and the expressed VAMP-2 eGFP fusion protein was distributed among a variety of different types of vesicles (Papini et al., 1995), including synaptic-like microvesicles (SLMV) and dense-core granules (DCGs) marked with secretogranin II. The presence of VAMP-2 and VAMP-2 eGFP in the pellet of the gradient is not surprising, since these proteins should also localize in endosomes, the plasma membrane, and other heavy subcellular structures.

Vesicle trafficking was imaged by illuminating a 5 × 5 μm area along a neurite of a PC12 cell and by monitoring the passage of fluorescent vesicles in *directed motion* across this window of observation, at a frame rate of 5 images/second (Fig. 2a). Representative trajectories are shown in Figure 2c with indicated times of observation. The size of the data points represents the accuracy of positioning the vesicle, to 35 nm from the sharp fluorescence peaks of each image, exemplified in Figure 2b. In this context, vesicle trajectories most likely represent a high-resolution image of cytoskeletal filaments. The flexible linkage of the vesicle to the filament via the motor-protein has a minor effect on this resolution (see Discussion for details). For reliable mapping of the filament network, it is necessary to acquire and compare trajectories from different vesicles. Figure 2c shows the trajectories of four vesicles which passed the same region of a neurite within 3 minutes. Two distinct pathways can be distinguished, indicated by gray lines in Figure 2d for an enlarged part of Figure 2c. The extremely precise match makes the statement highly reliable that the observed pathways represent the image of the underlying filament structure—a part of the full cytoskeletal network. Since the size of the observation window compares with the expected mean length of microtubules, ~4 μm (Yu and Baas, 1994), crossing-over events of vesicles between distinct pathways are expected. Indeed, the orange-colored trajectory in Figure 3 showed a transition between the two pathways.

The analysis of 83 trajectories permitted the quantification of basic characteristics of single vesicle motion during transport, summarized in Figure 3. Figure 3a shows that vesicle transport is abolished by treatment with nocodazole, a known microtubule-disrupting agent, supporting the notion that the observed transport along the neurite is mediated by microtubules, as expected. The observed velocities of *directed transport* (circles in Fig. 3b) had a mean value of $v_a = 0.68 \pm 0.27$ μm/s for anterograde transport (open circles) and of $v_r = 0.60 \pm 0.24$ μm/s for retrograde transport (filled circles). These mean values are in agreement with experiments using photobleaching (Nakata et al., 1998). The large widths of the distributions reflect a considerable variation of the velocity of each vesicle during transport.

Directed transport was generally interrupted by periods of local *diffusive motion* of vesicles, exemplified in Figure 2c (arrows). *Diffusive motion* is characterized by zero net velocity of the vesicles (see triangles in Fig. 3b) and a diffusion constant of $D = 3 \times 10^{-3} \mu m^2/s$. This mean value is in agreement with previous results obtained for mobility of secretory granules within the growth cone of PC12 cells (Abney et al., 1999). The time periods for *diffusive motion* were exponentially distributed with a mean duration of $\tau_d = 2.3$ s (see Fig. 3c), corresponding to a mean diffusive reach of 170 nm in all directions. Fluctuations perpendicular to the microtubule axis were especially largely enhanced during these periods. It is thus appropriate to ascribe such periods of diffusive motion to the dissociation of the vesicle from the filament. In addition, locations of *diffusive motion* showed no correlation for different trajectories and have been observed at random along the neurite and within the growth cone. This indicates that such transitions are not associated with structural features in the neurite, so that they are likely to reflect a property of the motor-vesicle complex itself. The durations of *directed transport* periods between locations of *diffusive motion* showed an exponential distribution with $\tau = 2.1$ s (see Fig. 3d), corresponding to a mean length of 1.2 μm, and with no resolvable difference for the two directions of transport. This built-in property of vesicle dissociation from the traveling pathway, followed by random diffusion and association to another pathway (for further examples, see Fig. 4), provides a solution to the need for many transitions between microtubules for long-distance vesicle transport. In general, the transport direction of individual vesicles was not affected by interruptions due to diffusive motion. Indeed, a reverse of active transport was never observed. Obviously, the motor protein responsible for the transport was not altered during the observation time.

Moreover, periods of diffusive motion appear instrumental also for mediating vesicle–vesicle interactions and further cotransport, as shown in Figure 4. One vesicle (green) was trapped at the beginning of the observation. A second vesicle (red) moved actively and met the first vesicle, upon which both vesicles moved on together. Eventually the two vesicles separated. One vesicle (red) continued *directed transport*. The other vesicle (green) entered a period of *diffusive motion* until it met another vesicle (blue) passing by in *directed transport* mode, with which it joined for further cotransport. In this example, *directed cotransport* of associated vesicles was characterized by a series of dissociation and reassociation events, suggesting a rather weak interaction, as illustrated in the data in Figure 4 by images taken at the indicated times.

Such association–dissociation events of two vesicles were subject to closer analysis (Fig. 5). The data in Figure 5a serve as a reference for studying vesicle association. It shows the probability distribution for the observed width σ of the image of single vesicles, yielding a mean value $\sigma_0 = 250$ nm. Association of vesicles will increase this value. However, movement also of a single vesicle out of the focal plane would yield a similar effect. Therefore, we recorded the vesicle motion in three dimensions and selected the proper focal plane for analysis. This is demonstrated in Figure 5b for 33 consecutive images. Three dissociation events are clearly discernable, two intermediate ones at 3.3 seconds, 6.3 seconds, and one at the end of the sequence. The characteristic time for dissociation-reassociation is estimated to be ~1 second.

Observations along the neurite were complemented by imaging vesicle transport in the growth cone. Its considerable extension along the optical axis required imaging in three dimensions. Figure 6 shows the entry of a transport vesicle into the growth cone and its pathway therein. At the beginning of the observation, the trajectory falls on a linear path of μm size, as expected for microtubule-mediated transport. Within the growth cone, the vesicle is transported along a highly curved route, not consistent with a series of μm-sized linear microtubule-based pathways. This observation suggests that vesicle transport within the growth cone may involve other structural elements, like actin filaments via myosin-based motor proteins

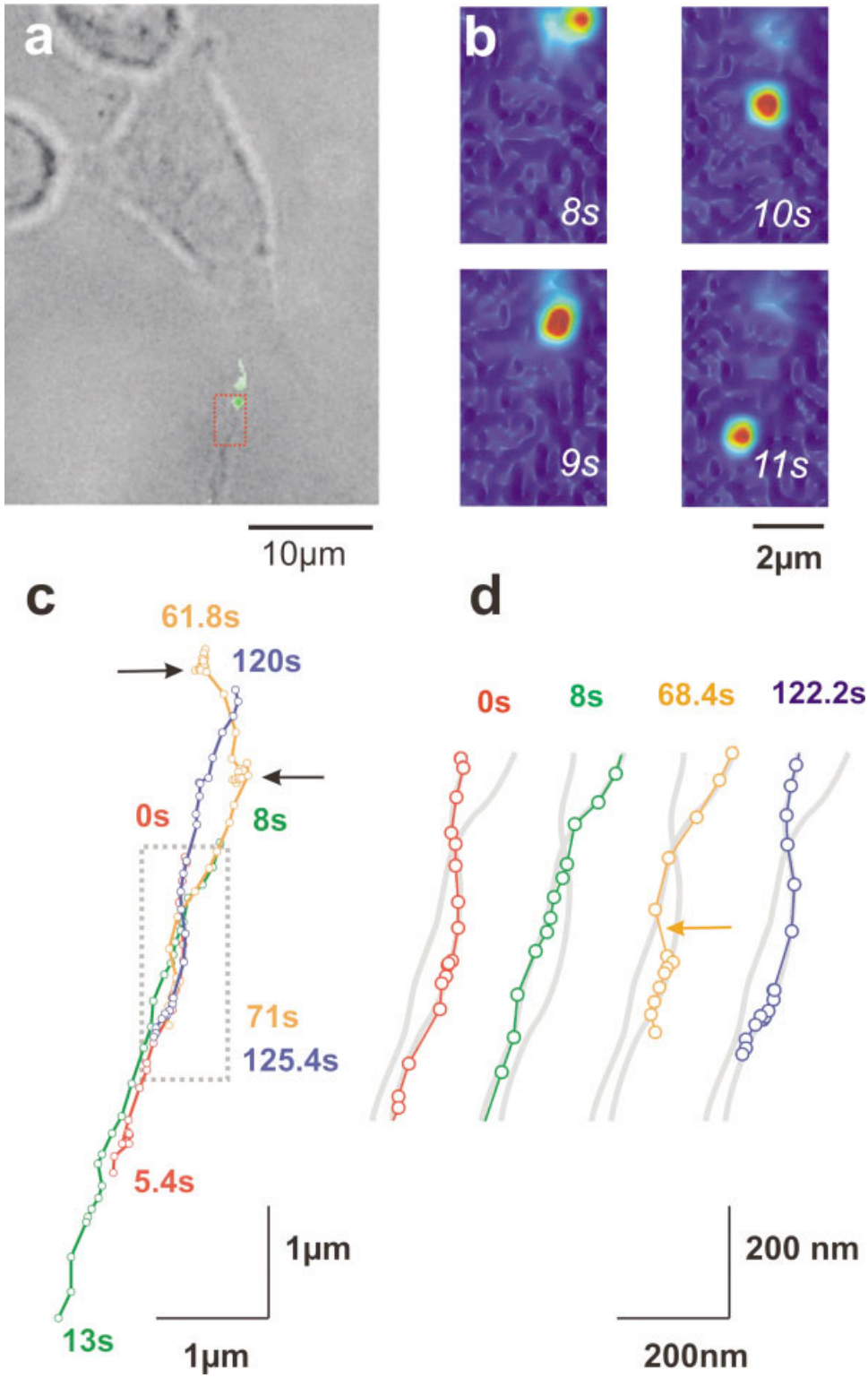

Fig. 2. Imaging of vesicle transport in two dimensions. **a:** Light image of a neuroendocrine (PC12) cell differentiated with nerve growth factor (NGF). This cell extends two neurites, one of which was chosen for subsequent fluorescence imaging within the window of analysis (red). **b:** Fluorescence image sequence over a period of 4 seconds. An individual vesicle can be observed as a sharp fluorescence peak as it is transported along the neurite in anterograde direction. **c:** An overlay of trajectories of individual vesicles observed within a time interval of 2 minutes. Two periods of diffusive motion are indicated by arrows. **d:** The four vesicles observed in **c** follow two distinct pathways, which most likely represent individual microtubule tracks, indicated by two gray lines of 30 nm width. While three of the vesicles (red, green, blue) stayed on the same path, one vesicle (orange) was observed to change from one pathway to the second (arrow). [Color figure can be viewed in the online issue, which is available at www.interscience.wiley.com.]

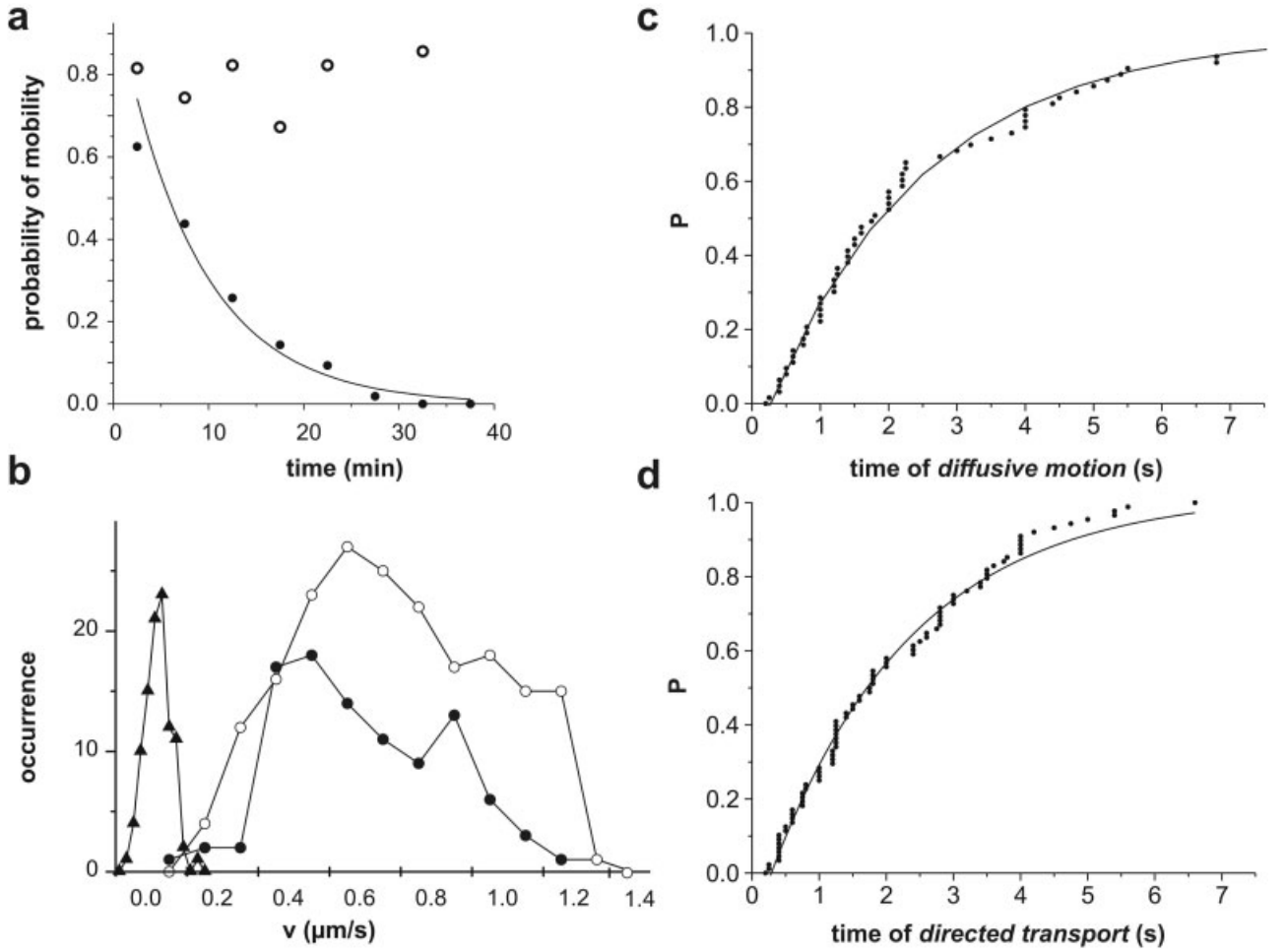

Fig. 3. **a:** Disruption of microtubules abolishes vesicle transport. The number of vesicles transported directionally decreased to zero after treatment of the VAMP2-eGFP PC12 cells with 20 μM nocodazole (Calbiochem, La Jolla, CA), a microtubule-disrupting reagent (solid symbols). The decay was fitted by an exponential function with a time constant of 8.4 minutes, which mainly reflects the kinetics of microtubule disruption. Without nocodazole treatment, no reduction was observed (open symbols). **b:** Statistical analysis of vesicle trajectories reveals different modes of motion. The histogram shows the distribution of velocities for anterograde (○) and retrograde (●) transport observed in 83 trajectories. For comparison, the apparent velocity within periods of diffusive motion is plotted (▲). **c:** Duration of diffusive motion in between periods of directed transport. For exponentially distributed times t, the distribution function is given by $P = 1-\exp(-t/\tau_d)$. Deviations from this relationship due to inaccuracies in discriminating short periods of diffusive motion were corrected by modifying the function to $P = (1-\exp(-t/\tau_d)) \times (1+\alpha)-\alpha$, with α describing the fraction of nonobserved periods of diffusive motion. The fit yielded $\tau_d = 2.3$ seconds. **d:** Duration of directed transport. The data follow an exponential distribution with $\tau = 2.1$ seconds.

(Dailey and Bridgman, 1991; Mermall et al., 1998; Ohyama et al., 2001).

DISCUSSION

In the present work, we studied the transport behavior of individual secretory vesicles within neurites at spatial and time resolutions sufficient to resolve details of processive motion and to follow vesicles during pathway changes. The high resolution required to study such mechanistic details was achieved by applying two- and three-dimensional fluorescence microscopy combined with automated fitting procedures.

In general, the high density of cytoskeletal filaments prevents direct imaging of fluorescently labeled actins and microtubules (Chang et al., 1999). Here, the pathways of individual vesicles were used to reconstruct a map of the underlying filaments. The obtained resolution of this map corresponds to the positional accuracy of the fitting algorithm, $\Delta x = 35$ nm, but also to the mechanical properties of the vesicle-motor protein–microtubule complex, Δd, according to $r = \sqrt{\langle \Delta x \rangle^2 + \langle \Delta d \rangle^2}$. Δd arises from the flexible linkage of the vesicle to the microtubule via the motor protein of length l. The average distance of the vesicle center from the microtubule axis is given by $d = l + \rho_v + \rho_m$, with ρ_v the vesicle radius, and ρ_m the microtubule radius. The length of motor proteins is well known from electron microscopy studies, yielding 80 nm and 45 nm for kinesin and dynein, respectively (Schliwa, 2003). The radius for secretory vesicles was assumed to be 75 nm for the microtubule to be 12.5 nm (Wagner, 1985). The maximum value of Δd would be obtained for a motor protein freely rotatable about its microtubule an-

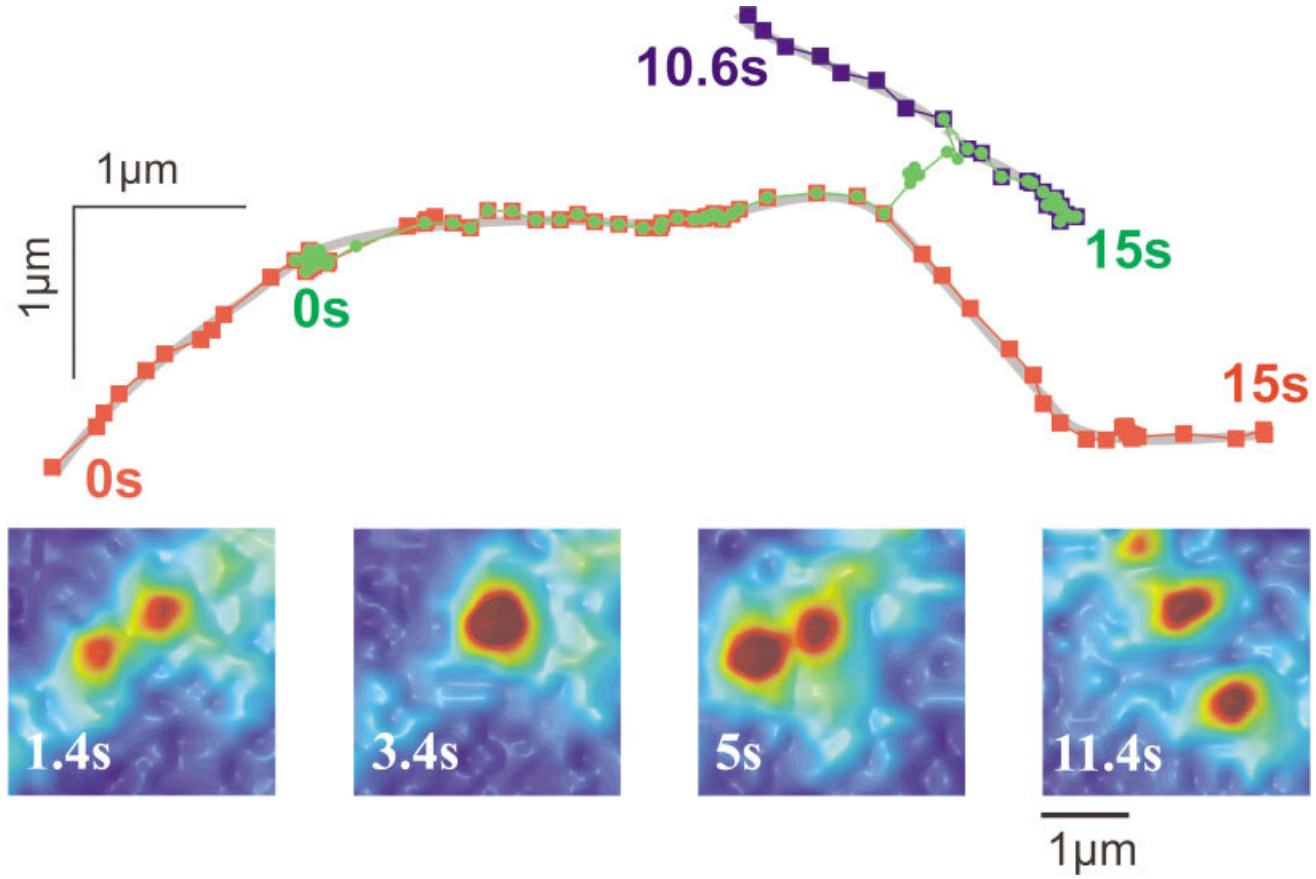

Fig. 4. Interaction of three vesicles during transport. The top shows the trajectories of three vesicles transported along the neurite. One vesicle was inactive initially (green trajectory), while the other was transported directionally to the first vesicle. Both remained inactive for 2.6 seconds before being transported together directionally. After an additional 6 seconds, the "green" vesicle left the common pathway and entered a period of diffusive motion for 1.2 seconds until it interacted with the "blue" vesicle for further directional transport. Four fluorescence images exemplify four distinct stages of the interaction process (left to right): before interaction, during the complex formation, shape fluctuations of the complex, and final separation. This observation most likely represents the indirect transport of a per se not motor-driven vesicle (green) via interaction with actively transported vesicles (red, blue). [Color figure can be viewed in the online issue, which is available at www.interscience.wiley.com.]

chor point, $\Delta d = \sqrt{\frac{1}{3}}\, d$. In total, the upper limit for the overall inaccuracy for mapping cytoskeletal filaments is given by $r \approx 103$ nm for kinesin and $r \approx 84$ nm for dynein. Experimental data obtained in motility assay in vitro showed even less side-flops of bead-labeled motor proteins moving along microtubules (Wang et al., 1995).

During transport, no reverses in the direction were observed. This finding obtained for transport of SLMVs in neurites is different from the transport behavior of organelles (Ma, 2002) and lipid droplets (Gross et al., 2000). It shows that either plus-end or minus-end directed motor proteins are activated on a single vesicle, even in periods of diffusive motion. While directionality was sustained, active transport was observed to proceed with large fluctuations in velocity. Changes in the local viscosity along the neurite due to steric hindrance (Holzwarth et al., 2002) and alterations of the activation state of the motor protein contribute to these variations.

Periods of diffusive motion have been ascribed to the dissociation of the vesicle from the microtubule, with subsequent Brownian motion of the vesicle in the cytoplasm of the neurite. Several lines of argument support this interpretation: First, the observed diffusive range of 170 nm exceeds the resolution r for mapping the microtubule axis. Second, the continuation of the transport after diffusive motion proceeds in general along a different filament (see, e.g., Fig. 4). Third, limited processivity of motor proteins is a well-known phenomenon in vitro (Block et al., 1990; Thorn et al., 2000), rendering the dissociation of vesicles highly plausible.

Continuous cargo transport from the cell body to the growth cone and back is therefore based on a sequence of processive motions along filaments with intermittent pathway changes. One remarkable finding in these studies was the limited, mean run length of kinesin which could be increased several fold by point mutations above the wildtype value of 1.5 µm (Thorn et al., 2000). This led to the suggestion that the kinesins run length may have been selected by evolutionary pressure to an optimum mean value, much below its possible maximum value. It is of interest that the processiv-

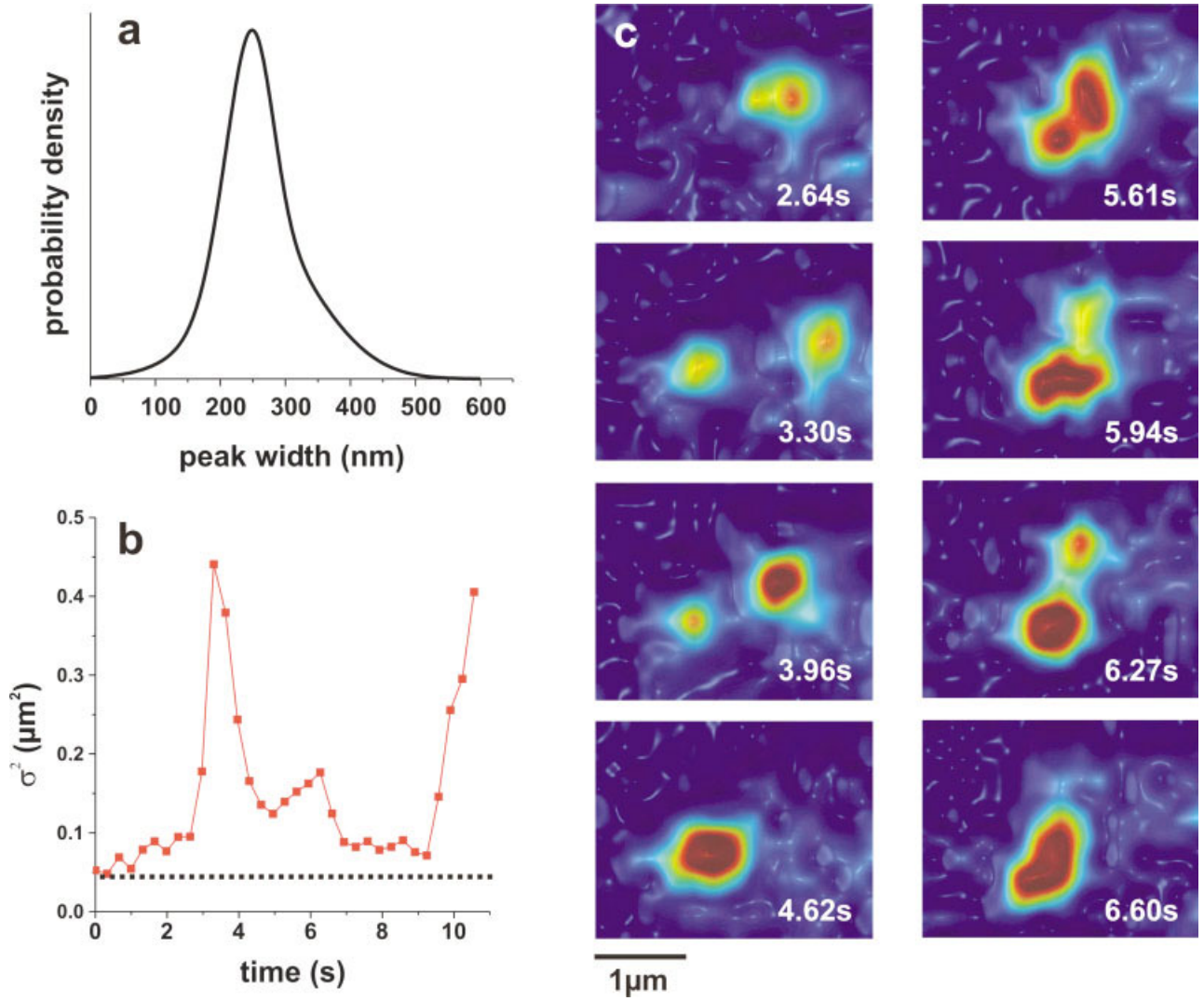

Fig. 5. Size fluctuations of vesicle complexes. **a:** Estimation of the size of a vesicle. The full width at half maximum of the signal of 15 vesicles was determined (see text for details), yielding a mean of 250 nm. This agrees well with the diffraction limited spot size of 232 ± 2 nm, indicating a vesicle size below 100 nm, in agreement with reported data (Linstedt and Kelly 1991). **b:** The width of the fluorescence signal, σ, as a measure of dissociation-association fluctuations. The large peak at about 3.3 seconds and the small peak at about 6.27 seconds correspond to the images shown in **c**. For comparison, the respective value for the diffraction-limited spot size, obtained on immobilized 30 nm latex spheres, is indicated as a dotted line. **c:** Eight images exemplifying different stages of a complex of two vesicles. For each time point, a series of four images was recorded within 70 ms utilizing the 3D imaging mode of the microscope. From each series the image closest to the plane of focus of the vesicle was selected for illustration. The complex of the two vesicles could not be distinguished from a diffraction-limited spot (4.62 seconds). Occasionally, however, dissociation lead to the separation of the vesicles to distances larger than the diffraction limit, so that both vesicles could be resolved as individual spots (3.3 seconds, 3.96 seconds). Between these extremes, distance fluctuations of the two vesicles were observed as shape fluctuations of the image (5.16–6.6 seconds). [Color figure can be viewed in the online issue, which is available at www.interscience.wiley.com.]

ity found here in the native context of a neurite, being exponentially distributed with a mean run length of 1.2 μm for both anterograde and retrograde transport, quantitatively matches the processivity properties of the in vitro wildtype kinesin (Thorn et al., 2000) and dynein (Wang et al., 1995). Since processivity scales with the number of associated motor proteins, our finding implies that only a single or a few motor molecules are involved in active transport of SLMVs.

The observed transient association of vesicles offers various ways for en route sorting of proteins along neurites. It was recently postulated that only part of the required proteins is targeted to the final destination via sorting signals, which are peptide domains specifically interacting with motor proteins. In that model, the remaining fraction, which lacks signals, is transported in a "piggyback style" by association with proteins containing sorting signals (Ahmari et al., 2000; Roos and Kelly, 2000). Such association was suspected to happen already in the Golgi, leading to stable transport packets. We find here a succession of association and dissociation events throughout transport

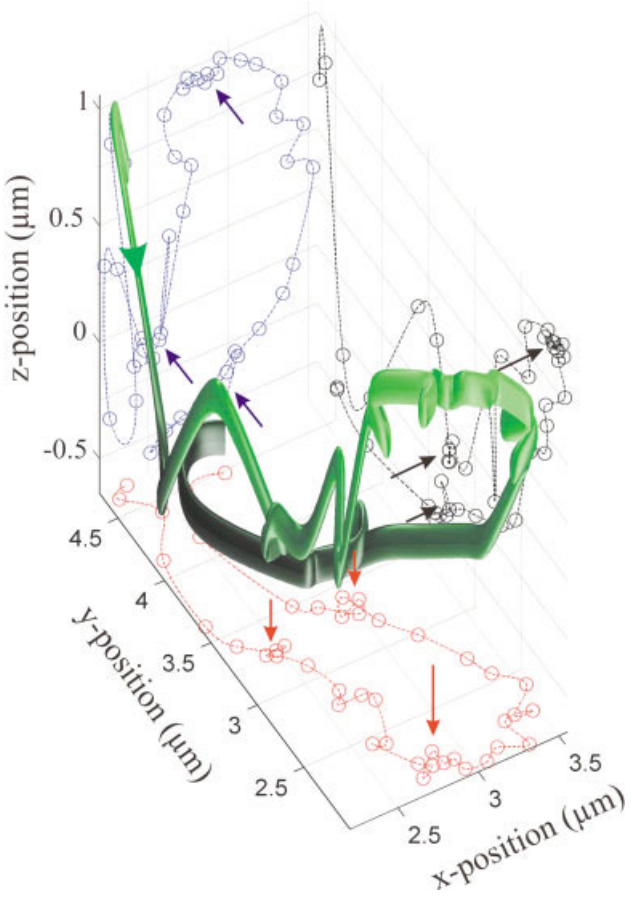

Fig. 6. The 3D trajectory of a single vesicle within the growth cone is shown as a green ribbon, with its dimensions resembling the positional accuracy (35 nm laterally, 75 nm vertically). The time resolution allows distinguishing periods of directed transport from periods of diffusive motion (indicated by arrows). For clarity, the projections of the trajectory onto the xy, xz, and yz plane are shown in red, blue, and black, respectively. In this example, the vesicle is transported out of the neurite into the growth cone and guided along the front face back towards the neurite. [Color figure can be viewed in the online issue, which is available at www.interscience.wiley.com.]

within the neurite, some of which indicate "piggyback transport" (Fig. 4). Such en route sorting enhances the flexibility of transport, thereby allowing fine adjustments for the final protein destination.

Outlook

The methodology presented here can now be extended to image the dynamics of vesicles in neurons in primary culture or in slices expressing VAMP2-eGFP and will allow multicolor imaging of either different classes of vesicles (SLMVs and dense core granules) or different components of the same class. It will be interesting to compare the dynamic picture presented here to the recently introduced concept of "prototerminals" (Ahmari et al., 2000). According to that model, components of presynaptic release sites in neurons have already been assembled before arriving at their target site. Our observations indicate a much more dynamic nature of vesicle packets, opening up the possibility for fine-tuning the composition of prototerminals during transport.

ACKNOWLEDGMENTS

We thank Vassili Pastushenko and Jörg Enderlein for mathematical assistance and Heike Kahr for keeping our cells warm.

REFERENCES

Abney JR, Meliza CD, Cutler B, Kingma M, Lochner JE, Scalettar BA. 1999. Real-time imaging of the dynamics of secretory granules in growth cones. Biophys J 77:2887–2895.
Ahmari SE, Buchanan J, Smith SJ. 2000. Assembly of presynaptic active zones from cytoplasmic transport packets. Nat Neurosci 3:445–451.
Allen RD, Metuzals J, Tasaki I, Brady ST, Gilbert SP. 1982. Fast axonal transport in squid giant axon. Science 218:1127–1129.
Block SM, Goldstein LS, Schnapp BJ. 1990. Bead movement by single kinesin molecules studied with optical tweezers. Nature 348:348–352.
Brady ST, Lasek RJ, Allen RD. 1982. Fast axonal transport in extruded axoplasm from squid giant axon. Science 218:1129–1131.
Chang S, Svitkina TM, Borisy GG, Popov SV. 1999. Speckle microscopic evaluation of microtubule transport in growing nerve processes. Nat Cell Biol 1:399–403.
Dailey ME, Bridgman PC. 1991. Structure and organization of membrane organelles along distal microtubule segments in growth cones. J Neurosci Res 30:242–258.
Goldstein LS, Yang Z. 2000. Microtubule-based transport systems in neurons: the roles of kinesins and dyneins. Annu Rev Neurosci 23:39–71.
Gross SP, Block SM, Wieschaus EF. 2000. Dynein-mediated cargo transport in vivo. A switch controls travel distance. J Cell Biol 148:945–956.
Hirokawa N. 1998. Kinesin and dynein superfamily proteins and the mechanism of organelle transport. Science 279:519–526.
Holzwarth G, David KB, Hill B. 2002. Forces required of kinesin during processive transport through cytoplasm. Biophys J 82:1784–1790.
Kobayashi N, Mundel P. 1998. A role of microtubules during the formation of cell processes in neuronal and non-neuronal cells. Cell Tissue Res 291:163–174.
Kuznetsov SA, Langford GM, Weiss DG. 1992. Actin-dependent organelle movement in squid axoplasm. Nature 356:722–725.
Lang T, Wacker I, Steyer J, Kaether C, Wunderlich I, Soldati T, Gerdes HH, Almers W. 1997. Ca2+-triggered peptide secretion in single cells imaged with green fluorescent protein and evanescent-wave microscopy. Neuron 18:857–863.
Lin RC, Scheller RH. 2000. Mechanisms of synaptic vesicle exocytosis. Annu Rev Cell Dev Biol 16:19–49.
Linstedt AD, Kelly RB. 1991. Synaptophysin is sorted from endocytotic markers in neuroendocrine PC12 cells but not transfected fibroblasts. Neuron 7:309–317.
Lippincott-Schwartz J, Roberts TH, Hirschberg K. 2000. Secretory protein trafficking and organelle dynamics in living cells. Annu Rev Cell Dev Biol 16:557–589.
Lochner JE, Kingma M, Kuhn S, Meliza CD, Cutler B, Scalettar BA. 1998. Real-time imaging of the axonal transport of granules containing a tissue plasminogen activator/green fluorescent protein hybrid. Mol Biol Cell 9:2463–2476.
Ma S. 2002. Cytoplasmic dynein-associated structures move bidirectionally in vivo. J Cell Sci 115:1453–1460.
Meldolesi J, Huttner WB, Tsien RY, Pozzan T. 1984. Free cytoplasmic Ca2+ and neurotransmitter release: studies on PC12 cells and synaptosomes exposed to alpha-latrotoxin. Proc Natl Acad Sci USA 81:620–624.
Mermall V, Post PL, Mooseker MS. 1998. Unconventional myosins in cell movement, membrane traffic, and signal transduction. Science 279:527–533.
Nakata T, Terada S, Hirokawa N. 1998. Visualization of the dynamics of synaptic vesicle and plasma membrane proteins in living axons. J Cell Biol 140:659–674.
Ohyama A, Komiya Y, Igarashi M. 2001. Globular tail of myosin-V is bound to vamp/synaptobrevin. Biochem Biophys Res Commun 280:988–991.
Papini E, Rossetto O, Cutler DF. 1995. Vesicle-associated membrane protein (VAMP)/synaptobrevin-2 is associated with dense core secretory granules in PC12 neuroendocrine cells. J Biol Chem 270:1332–1336.

Roos J, Kelly RB. 2000. Preassembly and transport of nerve terminals: a new concept of axonal transport. Nat Neurosci 3:415–417.

Scalettar BA, Rosa P, Taverna E, Francolini M, Tsuboi T, Terakawa S, Koizumi S, Roder J, Jeromin A. 2002. Neuronal calcium sensor-1 binds to regulated secretory organelles and functions in basal and stimulated exocytosis in PC12 cells. J Cell Sci 115: 2399–2412.

Schliwa M. 2003. Molecular motors. New York: Wiley-VCH.

Schütz GJ, Kada G, Pastushenko VP, Schindler H. 2000a. Properties of lipid microdomains in a muscle cell membrane visualized by single molecule microscopy. EMBO J 19:892–901.

Schütz GJ, Pastushenko VP, Gruber HJ, Knaus H-G, Pragl B, Schindler H. 2000b. 3D imaging of individual ion channels in live cells at 40nm resolution. Single Mol 1:25–31.

Sheetz MP. 1999. Motor and cargo interactions. Eur J Biochem 262: 19–25.

Taylor EW, Borisy GG. 2000. Kinesin processivity. J Cell Biol 151: F27–29.

Thorn KS, Ubersax JA, Vale RD. 2000. Engineering the processive run length of the kinesin motor. J Cell Biol 151:1093–1100.

Vale RD, Milligan RA. 2000. The way things move: looking under the hood of molecular motor proteins. Science 288:88–95.

Wagner J. 1985. Structure of catecholamine secretory vesicles from PC12 cells. J Neurochem 45:1244–1253.

Wang Z, Khan S, Scheetz MP. 1995. Single cytoplasmic dynein molecule movements: characterization and comparison with kinesin. Biophys J 69:2011–2023.

Yu W, Baas PW. 1994. Changes in microtubule number and length during axon differentiation. J Neurosci 14:2818–2829.